THE JOURNAL OF PHYSICAL CHEMISTRY B

Article

pubs.acs.org/JPCB

Femtosecond Two-Photon Ionization and Solvated Electron Geminate Recombination in Liquid-to-Supercritical Ammonia

Janus Urbanek, Annika Dahmen, Joel Torres-Alacan, Peter Königshoven, Jörg Lindner, and Peter Vöhringer*

Abteilung für Molekulare Physikalische Chemie, Institut für Physikalische und Theoretische Chemie, Rheinische Friedrich-Wilhelms-Universität, Wegelerstraße 12, 53115 Bonn, Germany

ABSTRACT: The first-ever femtosecond pump−probe study is reported on solvated electrons that were generated by multiphoton ionization of neat fluid ammonia. The initial ultrafast ionization was carried out with 266 nm laser pulses and was found to require two photons. The solvated electron was detected with a femtosecond probe pulse that was resonant with its characteristic near-infrared absorption band around 1.7 μm. Furthermore, the geminate recombination dynamics of the solvated electron were studied over wide ranges of temperature (227 K $\leq$ T $\leq$ 489 K) and density (0.17 g cm^{-3} $\leq \rho \leq$ 0.71 g cm^{-3}), thereby covering the liquid and the supercritical phase of the solvent. The electron recombines in a first step with ammonium cations originating from the initial two-photon ionization thereby forming transient ion-pairs (e_{am}^{-}·NH_4^{+}), which subsequently react in a second step with amidogen radicals to reform neutral ammonia. The escape probability, i.e., the fraction of solvated electrons that can avoid the geminate annihilation, was found to be in quantitative agreement with the classical Onsager theory for the initial recombination of ions. When taking the sequential nature of the ion-pair-mediated recombination mechanism explicitly into account, the Onsager model provides a mean thermalization distance of 6.6 nm for the solvated electron, which strongly suggests that the ionization mechanism involves the conduction band of the fluid.

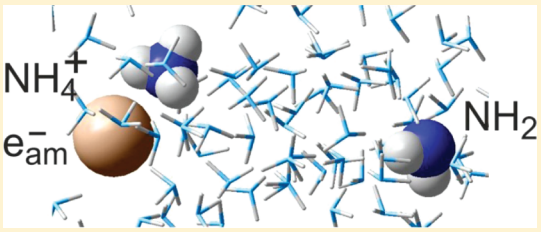

INTRODUCTION

In the recent decades, solvated electrons have raised considerable experimental and theoretical research activities, primarily devoted to understanding their spectroscopic properties, their reactivity, and their interactions with a molecular environment on ultrafast time scales. More specifically, coupled electron−solvent dynamics involve phenomena such as charge localization and delocalization, solvation and thermalization, or reactive and nonreactive electron−solvent scattering including charge transfer, all of which are important aspects in radiation chemistry.[1] The majority of the research devoted to time-resolving such dynamical processes focused on the solvated electron in liquid water[2] where it can be readily prepared via pulse radiolysis or laser-induced multiphoton ionization.

Historically, the solvated electron was first discovered in liquid ammonia (see e.g., ref 3 and references therein) where it can be prepared chemically by directly dissolving neat alkali metals into the solvent. However, the ultrafast electron−solvent dynamics in liquid ammonia are much less understood compared to those of the hydrated electron. This is because the preparation of metal-ammonia samples with long-term stabilities and linear optical properties that are suitable for dynamic spectroscopies is not at all trivial. Consequently, experimental studies employing time-resolved optical probing of the ammoniated electron in the bulk liquid are rather scarce.

Central to the existence of solvated electrons are questions related to the very nature of the binding motif of the excess charge to the molecular liquid environment.[4] Is the solvated electron best described as a polaron-like entity occupying a cavity structure within the liquid or is it more appropriately represented as a negatively charged and solvated cluster of molecules over which the total spin density is diffusely distributed?

To address this issue in a systematic fashion, experiments were first performed in supersonic expansions of NH_3. Haberland and co-workers were able to prepare and detect singly negatively charged ammonia clusters using mass spectrometry and to determine their cluster size distribution.[5] Shortly thereafter, photoelectron spectroscopy (PES) was conducted on size-selected negatively charged $(NH_3)_n^-$ clusters to determine the vertical detachment energy (VDE) as a function of the cluster size. By extrapolation, it was possible to determine the electron binding energy for infinitely large clusters, which in turn should correspond approximately to the photoelectric threshold energy (PET) for the bulk liquid (~1.25 eV), i.e., the minimum energy required to remove a fully thermalized solvated electron from the bulk liquid into the vacuum.[6,7] Photoionization experiments with a tunable laser were carried out by Schulz, Hertel, and co-workers on neutral ammonia clusters that were doped with a single atom of sodium.[8,9] The ion yield spectra were used to extract the ionization potential of the $Na(NH_3)_n$ species, which extrapolated for $n \rightarrow \infty$ roughly to the PET of liquid ammonia extracted from the PES experiments on $(NH_3)_n^-$.

Received: December 6, 2011
Revised: January 23, 2012
Published: January 24, 2012

Time-resolved spectroscopies on such gas-phase ammonia clusters were initiated by Schulz and Hertel, who developed femtosecond pump−probe spectroscopy with photoelectron-photoion coincidence detection thereby giving access to the dynamics in the excited states of neutral $(NH_3)_n$ species[10] and their sodium doped counterparts,[11] $Na(NH_3)_n$. For the metal−ammonia clusters, rates for energy redistribution from the sodium chromophore to the internal vibrations of the solvent molecules were retrieved as a function of the cluster size. While these dynamics occurred on a nanosecond time scale for a simple $Na-NH_3$ heterodimer, they accelerated drastically into the subpicosecond time scale upon adding additional ammonia molecules to the cluster. Finally, Zewail and co-workers carried out pump−probe PES on singly anionic $(NH_3)_n^-$ clusters and observed a 500 fs structural relaxation that was driven by the ultrafast optical excitation and the subsequent internal conversion back to the electronic ground state.[12] The body of these gas phase experiments has led to the general concensus that the size-selected clusters (either their undoped anionic forms or their Na-doped neutral forms) can be viewed as embryonic models of the ammoniated electron in the bulk liquid.[6,7]

As alluded to above, time-resolved spectroscopy on the ammoniated electron in the liquid phase is extremely difficult for technical reasons. Nevertheless, Huppert et al. as well as Belloni et al. reported independently on picosecond pump−probe measurements on metal-ammonia solutions more than 35 years ago.[13,14] Because of an insufficient time-resolution, it was impossible to accurately extract the coupled electron−solvent dynamics following a resonant optical excitation of the ammoniated electron. These remained the only studies until very recently, when our own group[15,16] was finally able to fully time-resolve the spectro-temporal evolution in the near-infrared spectral region of the ammoniated electron from metal-ammonia solutions by optically exciting it with femtosecond pulses at 1.3 μm. The data clearly revealed the quasi-prompt nature of an initial nonadiabatic transition that is followed by a subsequent thermal-structural relaxation of the coupled electron−solvent system within less than 200 fs.

Early theoretical work on the ammoniated system was initiated by Jortner who used a simple polaron model to understand the spectral position of the solvated electron resonance and its temperature dependence.[17] More refined path integral molecular simulations were then carried out by Barnett et al. as well as by Klein and co-workers to complement the experimental cluster studies[18−20] and to understand from an atomistic point of view structural and dynamical aspects of electron localization and solvation in ammonia.[21−26] Finally, using density functional theory, the adequacy of representing the ammoniated electron as a solvent stabilized multimer radical anion has been discussed in the context of nuclear magnetic resonance data.[27]

In this work, we present the first-ever experimental study of ammoniated electrons generated by femtosecond multiphoton ionization of bulk fluid ammonia. While multiphoton ionization has been used extensively to generate hydrated electrons and to investigate their ensuing chemical reactions,[28−41] no such photochemical data are available for ammoniated electrons. We will focus here on the ionization mechanism as well as on the dynamics of geminate recombination. A special emphasis is put on the so-called escape probability. This quantity is equal to the fraction of electrons initially created by the ionization pulse that is able to avoid a reactive encounter with the geminate counter fragments. The escape probability will finally be discussed in the framework of Onsager's classical theory for the initial recombination of ions.[42]

EXPERIMENTAL SECTION

The experimental setup was a slightly modified version of that used in a previous experiment[39] and will therefore be described only briefly. Femtosecond transient absorption measurements were carried out using a home-built 1 kHz Ti:sapphire regenerative chirped pulse amplifier as a front-end to an ultraviolet (UV)-pump and near-infrared (IR)-probe spectrometer. The front-end delivered 800 nm pulses with a duration of 150 fs and an energy of 750 μJ that were split by a 50% dielectric beam splitter. One part of the fundamental was frequency doubled in a 1 mm BBO crystal (type I), and the resulting second harmonic was then sum-frequency mixed with the residual fundamental in a 0.4 mm type I-BBO crystal to obtain 266 nm UV-pulses that were used for photoionization of fluid ammonia. The other 50% fraction of the front-end's fundamental output was used to pump an optical parametric amplifier (OPA, TOPAS, Light Conversion) to provide femtosecond near-IR pulses tunable between 1200 and 2400 nm. The signal (or idler) pulses of the OPA were divided by a dielectric beam splitter into probe and reference pulses, both of which were focused into the sample using a 45° off-axis aluminum mirror with a focal length of 100 mm. The pump beam was focused with a fused silica lens (400 mm focal length) and was spatially overlapped inside the sample with the probe pulses at an angle of 5°. The pump beam radius directly at the sample was 460 μm, whereas that of the probe beam was 240 μm. The pump pulse irradiance in front of the sample cell was roughly 30 GW/cm^2. After passing through the cell, probe and reference pulse intensities were detected by PbS-photoresistors whose electrical signals were fed into gated integrators. The pump could be adjusted by a combination of a half-wave retardation plate and a polarizer without changing the diameter of the beam and the probe beam was attenuated by neutral density filters.

We investigated the geminate recombination kinetics over a wide temperature and density range, as illustrated in the phase diagram of ammonia (see Figure 1). The experiments were

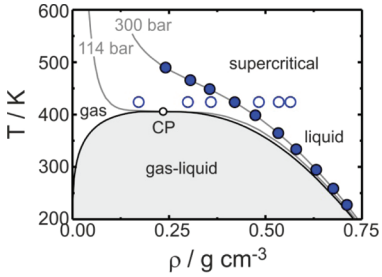

Figure 1. Phase diagram of ammonia. The gray-shaded area corresponds to the liquid−vapor coexistence region as defined by the liquid−vapor binodal (black solid curve). The gray curves display two representative isobars. CP is the critical point at 112.8 bar, 405.4 K, and 0.235 g/cm^3. The symbols represent the thermodynamic conditions at which kinetic experiments were carried out.

organized into a measurement series carried out along the 300 bar-isobar (see solid circles, Figure 1) and another one along the supercritical 423 K-isotherm (open circles). The pressure and temperature dependent density was calculated using the PROPATH program package.[43] The temperature and density dependent dielectric constant of ammonia was taken from ref 44.

Samples of pure NH_3 (99.98%, Linde) were prepared in a stainless steel high-temperature and high-pressure optical cell described in detail previously.[45−47] The entire high pressure system was purged with liquid CO_2 and subsequently evacuated to remove all traces of impurities such as water. The windows were cleaned with acetone prior to assembly of the cell. Its optical path length was 1.0 mm and 2.5 mm thick sapphire substrates were employed as windows. We upgraded the cell by an external cooling jacket to extend our measurements to cryogenic temperatures. No permanent photodamage or changes in the kinetics were observed upon continuously photolyzing the sample for several hours. Furthermore, the kinetics remained invariant to changes of the pump beam irradiance between 15 GW/cm^2 and 40 GW/cm^2. The recombination dynamics were recorded in a time window of altogether 800 ps in which 350 data points were acquired. At each data point, an average over 400 pump/probe cycles was calculated.

RESULTS AND DISCUSSION

Solvated Electron Formation and Decay. Irradiation of fluid ammonia with 266 nm light pulses generates a transient species that is characterized by a very broad absorption spectrum in the near-infrared (IR). As shown in Figure 2, this

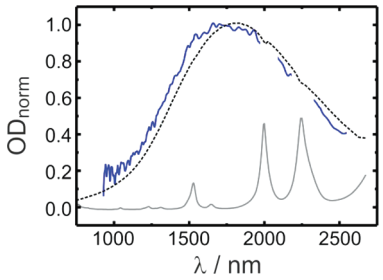

Figure 2. Comparison of the absorption spectrum of liquid ammonia upon 266 nm photolysis (solid curve, T = 295 K, p = 300 bar, ρ = 0.631 g/cm^3, recorded 400 ns after excitation) with an absorption spectrum of a metal-ammonia solution (dashed curve, T = 295 K, p = 9.07 bar, ρ = 0.608 g/cm^3, see ref 16). The gray curve represents a scaled absorption spectrum of the pure solvent, which is dominated in this spectral region by strong NH-stretching vibrational overtones and combination bands. The spectrum obtained by photolysis peaks at roughly 1760 nm, while that of the metal ammonia solution is maximal at 1820 nm. The small relative shift between the ammoniated electron absorption bands is due to the different pressure and density.

near-IR resonance is very similar in spectral shape and position to the linear absorption spectrum of solvated electrons that are generated chemically by dissolving an alkali metal such as sodium in liquid ammonia.[15,16] There can be no doubt that the species generated photolytically from the neat solvent at 266 nm carrying the strong and broad near-IR spectroscopic transition is identical to the chemically generated ammoniated electron from metal-ammonia solutions.

It is well-known that photoionization of neat liquids prepares excess electrons in a nonequilibrium configuration. The ensuing relaxation processes leading to a fully localized and thermalized solvated electron by structural rearrangements and thermal cooling of the solvent shell give rise to a dynamic blue shift of the solvated electron's optical resonance.[15,16,32,34] Therefore, the spectro-temporal evolution in the mid-to-near-IR at early times will inevitably contain contributions arising from these solvation and cooling dynamics. Such contributions can, however, be disentangled from the recombination kinetics by optically probing the system exclusively on the high-frequency edge or on the maximum of the stationary absorption spectrum of the solvated electron, i.e., by tuning the probe pulses to detection wavelengths that are shorter than or equal to the wavelength of maximal stationary absorbance of the solvated electron at the current temperature and density of the experiment.[39] In that case, thermal cooling and/or solvent reorganization can only result in a temporal rise of the absorbance, while a temporal decay is unequivocally related to a time-dependent loss of solvated electrons, i.e., to the decay of the solvated electron population by virtue of their recombination with reactive fragments in the fluid.

Therefore, prior to carrying out femtosecond experiments on the recombination dynamics, detailed information is required on the spectral position of the ammoniated electron's absorption band as a function of temperature and density. Fortunately, throughout almost the entire temperature and density range studied here, such data are available from experiments conducted by Schindewolf and co-workers many years ago.[48−50] Interestingly, at high temperatures and pressures, the stationary absorption of ammoniated electrons is reported to be barely sensitive to the thermodynamic conditions. At $T \geq$ 294 K, our probe wavelength was set to 1760 nm, whereas for lower temperatures the probe pulses had to be tuned to 1450 nm.

A representative pump−probe signal obtained by photoexcitation of neat ammonia with 266 nm pulses and probing in the near-IR at 1450 nm is shown in Figure 3 (top). Under all

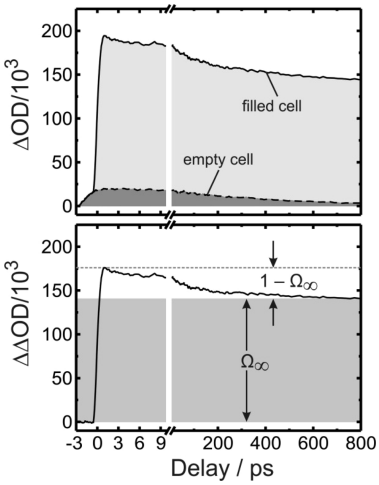

Figure 3. Top: Pump−probe signal of liquid ammonia (solid curve, p = 300 bar, ρ = 0.68 g/cm^3) and of the empty cell (dashed curve). The excitation wavelength was 266 nm, the probe wavelength was 1450 nm, and the temperature was 258 K in both cases. Bottom: Induced optical density difference, ΔΔOD, obtained from the two measurements. The escape probability, Ω_∞ (258 K, 0.68 g/cm^3) can be deduced from the maximal and long-time values of ΔΔOD.

conditions, the pump-induced optical density, ΔOD(t), consisted of an instrument-limited rise of a transient absorption that was followed by a slower decay. The observation of a temporally unresolved rise is consistent with a time constant of 150 fs for the relaxation dynamics that follow an optical (s-to-p type) excitation of fully thermalized solvated electrons in metal ammonia solutions.[15,16] The slower decay is indicative of the recombination loss of solvated electrons with increasing time delay. A careful inspection of the signal indicates that these

dx.doi.org/10.1021/jp211725r | J. Phys. Chem. B 2012, 116, 2223−2233

features were superimposed on an artifactual signal contribution, which we could unambiguously assign to a pump-induced absorption in the window of the sample cell. Therefore, for each pump−probe experiment on fluid ammonia, a second complementary experiment had to be carried out on the emptied cell. The undistorted response of the ammoniated electron, $\Delta\Delta OD(t)$, was then retrieved by simply subtracting the two data sets as demonstrated in Figure 3 (bottom). This approach is identical to that applied previously in our study of the geminate recombination of solvated electrons in liquid-to-supercritical water.[39] A peak amplitude of this window component of ~10% relative to the electron contribution was seen regardless of the probe wavelength used for the experiment. Note that the window contribution was also much smaller than in our previous studies on the hydrated electron.[39] Finally, the quality of the subtraction procedure can be assessed from the rising edge of the pure electron signal (cf. Figure 3, bottom).

It is also important to emphasize at this point that the focus here is solely on the peak signal amplitude, which is directly linked to the ionization mechanism, and on the decay of the signal, which is exclusively related to the loss of solvated electrons due to recombination reactions. The highest pump-induced optical density ever observed in our experiments was 0.16. Using an extinction coefficient of the solvated electron in ammonia[51] of 4.9×10^4 M^{-1} cm^{-1}, an average concentration of 3.5×10^{-5} M can be estimated. Furthermore, the decay seen in Figure 3 occurs on a time scale below 1 ns. On such short time scales and at such low concentrations, the apparent recombination dynamics are undoubtedly geminate in nature. This is further supported by the long-time plateau of the pump-induced optical density. In other words, the electron reacts with fragments that originate from the same ionization site. A fraction of solvated electrons is, however, able to escape from this initial annihilation and to diffuse away into the bulk. This fraction represents a solvated electron population that appears quasi-stationary on the subnanosecond time scale of the experiment and becomes apparent as an asymptotic pump-induced absorption for long pump−probe delays. Nongeminate recombination of solvated electrons in liquid ammonia is temporally very well separated from the geminate recombination and occurs in a homogeneous second-order reaction on time scales well in excess of 1 ns extending even into the microsecond regime.[52−55]

Geminate recombination is commonly characterized by the time-dependent survival probability, $\Omega(t)$, that corresponds to the fraction of solvated electrons still being present at a time, t, subsequent to the ionization event at $t = 0$. Assuming that the recombination and thermal equilibration dynamics are sufficiently separated in time, $\Omega(t)$ is immediately obtained from the ratio of the time-dependent induced absorption, $\Delta\Delta OD(t)$, to the peak induced absorption at early delays, $\Delta\Delta OD_{max}$. The asymptotic limit of this ratio for long pump−probe delays is accordingly referred to as geminate escape (or survival) probability, Ω_∞, as shown in Figure 3.

Photoionization Mechanism. To understand the photophysical processes responsible for the appearance and subsequent disappearance of solvated electrons following the UV irradiation of ammonia, it is of paramount importance to establish the number of photons involved in the primary matter-field interaction. The concentration of photolytically generated electrons is expected to increase with the n-th power of the pump irradiance where n photons simultaneously interact with the medium in the rate-limiting ionization step.[31] To establish this number, n, for the 266 nm photoionization of ammonia, the peak value of the induced optical density, $\Delta\Delta OD_{max}$, was determined for various pump pulse irradiances, I, at the sample. The peak induced optical density is a direct measure of the initially prepared solvated electron concentration prior to recombination and is unaffected by the solvation and thermalization dynamics.

Figure 4 displays a double-logarithmic representation of $\Delta\Delta OD_{max}$ as a function of I, where the irradiance is normalized

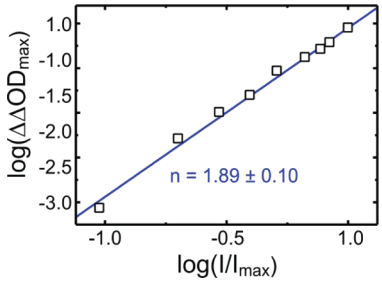

Figure 4. Dependence of the induced absorption of the ammoniated electron on the normalized pump-pulse intensity in a double-logarithmic plot. The data were recorded at a temperature of 294 K and a density of 0.63 g/cm^3. The straight line corresponds to a linear fit with a slope of 1.89.

to a value of 40 GW/cm^2 corresponding to the maximum pump intensities achieved in our experiments. The data closely follow a straight line having a slope of 1.89 ± 0.10, indicating that the photoejection process requires two photons, i.e., the matter-field interaction is a two-photon ionization. Two simultaneous photons with a wavelength of 266 nm have a total ionization energy of 9.3 eV. The slight deviation from the ideal slope of 2 can be attributed to inaccuracies of the correction for the window artifact, which becomes increasingly difficult with diminishing irradiance.

The electronic structure of polar liquids like water and ammonia can be understood conceptually in terms of a lone-pair amorphous semiconductor[56,57] in which short-range orientational order permits the merging of intermolecularly interacting nonbonding orbitals into a completely filled valence band. The latter is separated by a large energy gap from the conduction band, i.e., a continuum of quasi-free states, in which excess electrons are delocalized over many molecules in the liquid network.[56,57] A detailed discussion of the energetics relevant to the formation of solvated electrons is given by Bowen and co-workers[58] as well as Elles et al.[59] for the specific case of water.

In bulk liquid H_2O, the VDE corresponding to the most probable transition energy from the valence band to the ionization continuum is reported[60] to be 11.1 eV, while the photoelectric threshold, PET, corresponding to the minimal energy at which there is a sufficient spatial wave function overlap allowing for the detection of photoelectrons is 9.9 eV.[36] Vertical photoionization and vibrationally assisted autoionization of water[30] at such energies generate initially electrons within the conduction band, which delocalize on a time scale of less than 500 as.[61] Asymmetric or broken hydrogen-bond geometries present trapping sites for the electron, thereby serving as precursors for the fully solvated hydrated electron. Consistent with the delocalized nature of conduction band electrons, the average distance migrated before the electron becomes fully localized and thermalized is denoted ejection length (or equivalently,

thermalization distance). At such excitation energies, it is typically of the order of 4 nm in water.[31,62,63]

However, energies as low as 6.5 eV have been reported in the literature as threshold for the production of hydrated electrons in the bulk liquid, i.e., well below the PET.[64,65] Apparently, the photoinduced generation of solvated electrons can also involve solvent nuclear motions thereby bypassing the conduction band. Currently, a proton-coupled electron transfer and the ballistic hot H-atom mechanism are discussed.[30,37,39,41,65] Both mechanisms result in much smaller ejection lengths of around 1 nm.[36,41]

For ammonia, the energetics are significantly different.[66] All of the ammonia electronically excited states are of Rydberg character due to the promotion of an electron from the highest occupied lone-pair orbital connected with a geometry change from pyramidal (C_{3v}) to planar (D_{3h}). As a result, the absorption bands of ammonia in the gas phase are dominated by pronounced progressions in the ν_2 umbrella mode of NH_3.[67,68] The lowest excited state ($\tilde{A}^1A''_2$) has its origin at 5.74 eV, and is, like many of the other excited states, predissociative leading predominantly to ground state NH_2 ($\tilde{X}^2B_1$) and hydrogen atoms.[69] The VDE of an isolated molecule in the gas phase is 10.85 eV;[70] however, the adiabatic ejection of a photoelectron into the vacuum is possible via autoionization down to 10.07 eV.[71,72]

Experimental data pertaining to the energetics of the condensed phases of ammonia are scarce. In a theoretical study comprising sequential molecular dynamics simulations and density functional theory, Almeida et al. estimated the VDE of the liquid to be (9.7 ± 0.7) eV.[73] The energetic lowering of about 1 eV on entering the liquid was attributed to polarization effects and hydrogen bonding. A more reliable value for the VDE of 9.4 eV has been deduced from a recent photoelectron spectrum by Lindblad et al. on large ammonia clusters, $(NH_3)_n$, with a mean size of $n \approx 1600$ molecules/cluster.[74] Their spectrum also provides an upper limit for the PET of roughly 8 eV. If one takes into account a polarization-induced stabilization of the excess electron in the conduction band of ammonia of about 0.2 eV relative to the vacuum (i.e., similar to water, see ref 75), one arrives at a VDE of about 9.2 eV and at an upper limit for the onset of direct ionization of approximately 7.8 eV in the condensed phase. Of course, this estimate assumes that the existing cluster data are already converged to the true bulk phase values.[7,73]

Here, we report on ammoniated electrons that were generated photolytically using 266 nm laser pulses. The pump intensity dependence of the solvated electron's induced absorption indicated that the total photoionization energy in our experiments is 9.3 eV corresponding to two photons at 266 nm. This energy is very similar to the above estimate for the most probable transition energy for a vertical ionization of the fluid and certainly exceeds the above estimate of the PET of ammonia. Consequently, one can conclude that the underlying mechanism for photoejection is either direct vertical ionization or autoionization, both of which involve the intermediate formation of conduction band electrons having a delocalized character. There is no need for invoking mechanisms that bypass the conduction band as in the case of water for ionization energies below the band gap.

The hole remaining at the ionization core is an ammonia cation, NH_3^+, which has been reported to rapidly transfer a proton in the gas phase to a neutral ammonia molecule thereby forming an ammonium cation, NH_4^+, and the amidogen radical, NH_2.[76] The net result of the photoexcitation process is thus

$$2NH_3 + 2h\nu \rightarrow e_{am}^- + NH_2 + NH_4^+ \quad (1)$$

in correspondence to ref 54 and in analogy to water, where the photoionization at 9.3 eV generates hydroxyl radicals and hydronium cations as side products. Whereas the two primary molecular fragments will be produced in close proximity to the ionization site in the fluid, the electron will become localized at a remote location due to its intrinsic high mobility as a conduction band electron. Quasi-free electron states in polar media have been investigated in dense vapors, where excess electrons do not become solvated but prevail as highly mobile, delocalized species. On the basis of these results, the mobility of excess electrons in ammonia is significantly larger than in water at the same temperature.[77] Recalling the ejection lengths in water for ionization energies above the VDE,[36] thermalization distances in excess of 4 nm can be expected for solvated electrons generated in ammonia by two-photon-ionization at 266 nm.

Temperature and Density-Dependent Geminate Recombination. A representative selection of the pump−probe traces obtained at different thermodynamic conditions is presented in Figure 5. To facilitate a comparison, the induced

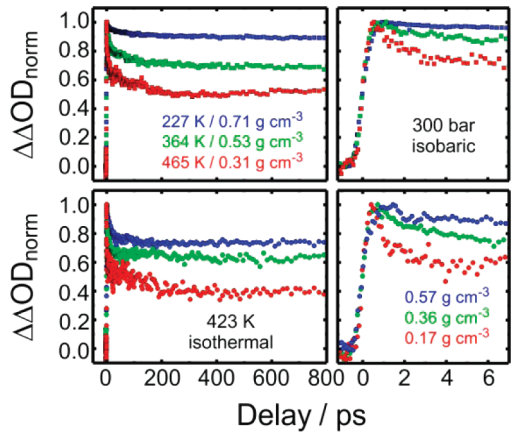

Figure 5. Temperature and density dependent kinetic traces of the ammoniated electron recorded along the 300 bar isobar (top panels) and along the 423 K isotherm (bottom panels). The probe wavelength was 1450 nm for 227 K and 1760 nm for 364 and 465 K, respectively.

absorption was normalized to its peak value and is hereafter referred to as $\Delta\Delta OD_{norm}(t)$. As before, all traces exhibit the instrument-limited rise at early times indicating that the primary thermalization dynamics of the solvated electron retain their subpicosecond character throughout the entire thermodynamic range covered in this work, i.e., from the dense cryogenic liquid all the way up to the dilute supercritical fluid. Furthermore, it can be seen that the subsequent decay of $\Delta\Delta OD_{norm}(t)$ to its asymptotic offset is complete within several 100 ps; however, it appears as if the decay is accelerated upon increasing the temperature or decreasing the density. This finding is consistent with our recent report on the geminate recombination dynamics of the solvated electron in liquid-to-supercritical water.[39]

From each individual kinetic trace, the geminate escape probability was calculated as an arithmetical mean of $\Delta\Delta OD_{norm}(t)$ over the delay interval between 400 and 800 ps. At a temperature of 227 K and a solvent density of 0.71 g/cm^3, the escape probability, Ω_∞, assumes a value of 89%, i.e., only 11% of the initially produced electrons are able to recombine in a geminate fashion. Upon isobarically heating the sample, the escape probability decreases markedly to 76% at 294 K and assumes a value of only 45% at a supercritical temperature of

dx.doi.org/10.1021/jp211725r | J. Phys. Chem. B 2012, 116, 2223−2233

489 K. Note that this temperature rise by about a factor of 2 is accompanied by a reduction of the solvent density of roughly a factor of 3. To disentangle in a systematic fashion, the density dependence of the escape probability from the temperature dependence, a complementary series of pump−probe experiments was conducted along the supercritical 423 K isotherm (see Figure 5, bottom row) thereby allowing for a variation of the density by more than a factor of 3. Again, the value of Ω_∞ decreases from 73% at a density of 0.57 g/cm^3 to about 40% at an almost vapor-like density of 0.17 g/cm^3. The complete temperature and density-dependence of the escape probability is summarized in Figure 6.

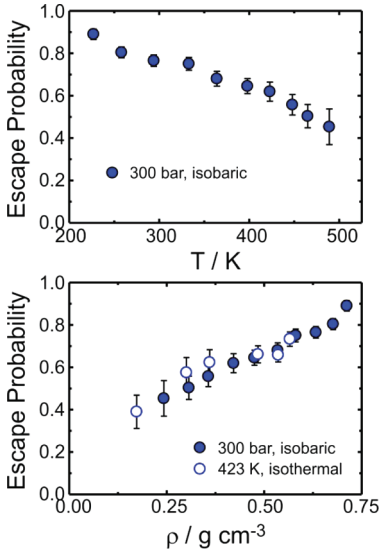

Figure 6. Temperature (top panel) and density (bottom) dependence of the escape probability for solvated electrons generated by 266 nm two-photon ionization of neat ammonia.

At the highest densities ($\rho \geq 0.7$ g/cm^3), a very large fraction of ammoniated electrons of up to 90% is able to escape from geminate recombination. For comparison, in liquid water, the highest escape yields of hydrated electrons ever observed at an ionization energy of 9.3 eV were only about 70%.[35] Although at a higher temperature (600 K), survival probabilities even as low as 15% have been detected in water at similar densities around 0.7 g/cm^3.[39] The dynamics of geminate recombination of solvated electrons in fluid ammonia subsequent to photoionization has not been studied so far. However, a number of nanosecond pulse radiolysis experiments[53−55,78−83] have been reported according to which the decay of the ammoniated electron can be traced back exclusively to the reaction with the amidogen radical,

$$e_{am}^- + NH_2 \rightarrow NH_2^- \quad (2)$$

Reaction 2 was found to be diffusion-controlled.[52,84] In other words, the reaction of the solvated electron with NH_2 radicals under formation of the amide anion features no significant energy barrier, and consequently, every encounter between the two particles is reactive. In this case, the temperature and density dependence of the reaction rate is governed by the diffusion coefficients of the recombining particles. Nevertheless, an anomalously large primary electron yield was reported,[78,79] which was attributed to the poor efficiency of the alternative recombination pathway

$$e_{am}^- + NH_4^+ \rightarrow NH_3 + H \quad (3)$$

This interpretation was further corroborated by a stopped-flow measurement of the kinetics of the reaction 3 using solvated electrons from a metal ammonia solution on the one hand and ammonium cations from a solution of NH_4Br in liquid ammonia on the other.[85] At 223 K, the measured second-order rate constant for reaction 3 is 1.2×10^6 M^{-1} s^{-1}, which is several orders of magnitude smaller than the calculated diffusion limit of 5.0×10^{11} M^{-1} s^{-1}.[52,85] A lower limit for the reaction barrier can be estimated from thermochemical data published by Schindewolf[86] according to whom the reaction enthalpy for reaction 3 is +30 kJ/mol, while the reaction entropy is −12 J/mol K. Thus, the charge neutralization is not only endothermic but in the temperature range studied here, also endergonic by at least 33 kJ/mol! Therefore, the charge neutralization reaction can safely be neglected.[84]

Our finding of surprisingly large escape probabilities as compared to water is in qualitative agreement with these early radiolysis studies. However, the pronounced dependence of Ω_∞ on temperature and density seemingly contradicts the conclusions from ref 79 according to which the radiolytical yield is more or less insensitive to temperature changes along the liquid branch of the liquid−vapor binodal between 198 and 296 K (i.e., for the liquid held under saturation pressure). The apparent contradiction between photolysis and radiolysis is most likely due to the different ionization conditions. Pulse radiolysis with badly defined ionization energies above hundreds of keV is well-known to yield significantly broader spatial electron distributions[1] as well as molecular radicals and ionic fragments from secondary spur reactions[87] that cannot occur in multiphoton ionization at a well-defined energy. Therefore, it might not be so surprising that the recombination kinetics of these two distinct approaches differ with respect to their dependence on the thermodynamic state variables.

Although the ammonium cation does not directly annihilate the ammoniated electron, it enhances the diffusional drift of the electron toward the dipolar radical. This is because shortly after ionization, the two geminate fragments, NH_2 and NH_4^+, are still in close spatial proximity, while the electron is located farther away due to the involvement of the solvent's conduction band during ionization. Whereas the reactivity of the electron is essentially defined through its interaction with the dipole, its diffusional drift is governed by the interaction with the cation simply because at any given separation, the Coulomb attraction between e_{am}^- and NH_4^+ outweighs the charge-dipole attraction between e_{am}^- and NH_2. Furthermore, the latter interaction is likely to be obscured by the presence of the overwhelming ammonia solvent dipoles. Consequently, the geminate recombination processes should be described more adequately by the following sequence of events:[80]

$$e_{am}^- + NH_4^+ \rightleftharpoons (e_{am}^- \cdot NH_4^+) \quad (4)$$

$$(e_{am}^- \cdot NH_4^+) + NH_2 \rightarrow NH_2^- + NH_4^+ \quad (5)$$

The existence of ion-pairs, $(e_{am}^- \cdot NH_4^+)$, has been deduced from early studies of the absorption spectrum of solvated electrons in metal-ammonia solutions and its dependence on the sample composition.[88] Jou and Freeman[89] have compared such concentration-dependent spectra with those obtained from

pulse radiolysis and concluded that the formation of the ion-pair does not alter the electronic resonance significantly. Therefore, the direct recombination of the ammoniated electron with the amidogen radical according to reaction 2 and the consecutive recombination following reactions 4 and 5 are indistinguishable by optical absorption spectroscopy.

Comparison with Onsager's Escape Probability. In the absence of external forces, the probability for two ions of opposite charge overcoming their mutual Coulomb attraction, $V(r_0)$, by thermal excitations at the temperature, T, is given by the reciprocal of the Boltzmann factor[42]

$$\Omega_\infty(r_0) = \exp[V(r_0)/k_BT] = \exp(-r_c/r_0) \quad (6)$$

where r_0 denotes the initial separation, and k_B is Boltzmann's constant. The Coulomb energy, $V(r_0)$, is equal to the thermal energy, k_BT, at the Onsager radius, $r_c = e^2/(4\pi\varepsilon\varepsilon_0 k_BT)$, when the solvent continuum has a dielectric permittivity of ε relative to that of the vacuum, ε_0. Notice that the escape probability depends not only on the temperature explicitly but also in an implicit fashion through the temperature dependence of the solvent's dielectric constant. Furthermore, even at constant temperature, ε is also a function of the density of the solvent. Taken together, $\varepsilon = \varepsilon(T,\rho)$ and Onsager's geminate escape probability in eq 6 should be written more appropriately as $\Omega_\infty = \Omega_\infty(r_0,\rho,T)$. Qualitatively, the theory predicts a decreasing recombination efficiency associated with an increasing free ion yield as the temperature is raised. Conversely, as the dielectric constant is lowered, the solvent screening of the attractive interionic forces is diminished, and the recombination becomes increasingly effective, which in turn leads to smaller free ion yields.

Equation 6 is based on the 2-fold assumption that the charge annihilation occurs instantly when the relative ion separation becomes zero. In the past, the Onsager model has been refined by several groups, most notably by Tachiya and co-workers,[90−92] to account for the fact that the recombination event corresponds to a charge transfer reaction. This requires the introduction of a finite reaction rate and of a finite reaction radius, R, with/at which the charge can actually be transferred back. To make use of eq 6 and to calculate an experimental observable, the escape probability has to be averaged over the distribution, $f(r_0)$, of initial separations of ion-pairs constituting the ensemble, i.e., $\langle\Omega_\infty\rangle = 4\pi\int r_0^2 f(r_0)\Omega_\infty(r_0)dr_0$.

In an effort to analyze pulse radiolysis data on different liquids, various functional forms have been proposed for $f(r_0)$ including exponentials, Gaussians, truncated Gaussians, or power laws. For photolytically generated hydrated electrons, it was shown that the detailed functional form is not so crucial because of the superior definition of the ionization energy in multiphoton ionization experiments as compared to pulse radiolysis. Indeed, numerical simulations using the delta-functional form, $f(r_0) = \delta(r_0 - \langle r_0\rangle)$, where $\langle r_0\rangle$ is the average ejection length (or thermalization distance), are able to reproduce the experimentally observed hydrated electron recombination dynamics very well.[41] Therefore, we will omit in the following an averaging over the detailed spatial distribution of fragments around the solvated electron and use the delta-function instead for describing the geminate survival probability. This leaves the ejection length, $\langle r_0\rangle$, as the only adjustable parameter for fitting the dependence of the experimental values of Ω_∞ on the thermodynamic state variables, T and ρ.

Following eq 6 strictly, the survival probability determined from the experimental pump−probe transients as described above is plotted in Figure 7 as a function of the density-dependent dielectric constant[44] multiplied by the temperature. To facilitate a comparison with other solvents, it is advantageous to reduce the quantity, $\varepsilon(T,\rho)T$, to the critical data, i.e., by dividing it by the product of $(\varepsilon T)_{crit} = \varepsilon(T_{crit},\rho_{crit})T_{crit}$ at the critical point, where for the special case of ammonia T_{crit} = 405.4 K, ρ_{crit} = 0.235 g/cm^3, and $\varepsilon(T_{crit},\rho_{crit})$ = 4.7. The bottom panel of Figure 7 corresponds to a semilogarithmic plot of the escape probability as a function of the inverse of the totally reduced product, $\varepsilon T/(\varepsilon T)_{crit}$.

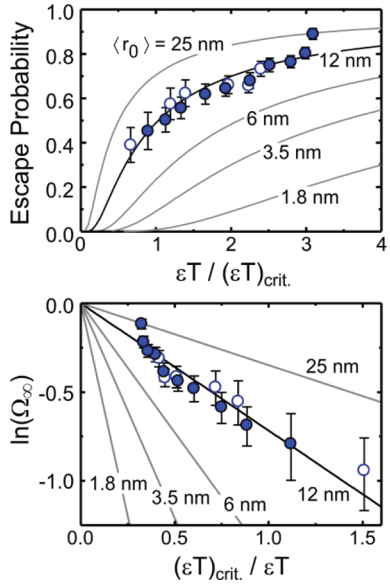

Figure 7. Experimental escape probabilities of the solvated electron in liquid-to-supercritical ammonia (filled circles, isobaric at 300 bar; open circles, isothermal at 423 K) as a function of the totally reduced product of the relative solvent permittivity and the temperature. For comparison, the prediction of the Onsager model according to eq 6 is also shown (solid curves) for various average ejection lengths. The Onsager radius varies between 2.8 nm (at 227 K and $\varepsilon T/(\varepsilon T)_{crit}$ = 3.1) and 13.2 nm (at 423 K and $\varepsilon T/(\varepsilon T)_{crit}$ = 0.67).

From both panels, it can be seen that within the accuracy of the experiment, the Onsager model is able to quantitatively reproduce the data. Furthermore, the data are optimally fitted when a mean thermalization distance of ∼12.2 nm is assumed. An average ejection length of around 12 nm is indeed very large. Notice that a thermalization distance around 1 nm was found for photolytically generated hydrated electrons in water at the same ionization energy of 9.3 eV used here.[93] The discrepancy can be rationalized by the different energetics in the two systems as described above. At 9.3 eV, the conduction band is accessible only in ammonia thereby creating highly mobile electrons that become trapped at locations far away from the initial ionization site. Therefore, the order-of-magnitude larger value of $\langle r_0\rangle$ as compared to water is indeed in very strong support of our above hypothesis of an ionization mechanism requiring the solvent conduction band.

A slight residual curvature of the experimental data points in the linearized representation (Figure 7, bottom panel) might indicate that the ejection length weakly increases as the temperature is isobarically raised or the density is isothermally reduced. In fact, there is no physical rationale justifying the assumption of a thermalization distance that does not vary with the thermodynamic conditions. It could very well be that upon

dx.doi.org/10.1021/jp211725r | J. Phys. Chem. B 2012, 116, 2223−2233

altering the interparticle distances, the interactions between the nonbonding orbitals leading to the formation of a conduction band change, and as a result, the average migration distances of an intermediate conduction band electron also vary. As the data were recorded in the vicinity of the critical point, further complications may arise due to local density enhancement effects.[94] Qualitatively, one would expect the orbital overlap to deteriorate as the density is isothermally decreased and the dielectric constant is lowered. This would actually lead to a decreasing ejection length with decreasing εT, and as a result, the data should exhibit a negative curvature in the $\ln(\Omega_\infty)$ versus $1/\varepsilon T$ plot. Such a behavior can, however, not be confirmed.

Onsager's Escape Probability for Ion-Pair-Dipole Recombination. Although the Onsager prediction matches our experimental data nicely, an application of the underlying model to the recombination of ammoniated electrons neglects the chemical nature of the annihilation mechanism. As discussed above, the actual loss of e_{am}^- occurs through their reaction with the dipolar radical, NH_2, rather than with their ammonium counterion. Therefore, we are dealing primarily with a reaction involving dipoles and not exclusively with an ion−ion recombination for which the theory was originally developed.[42,90]

The Onsager model would describe the escape probability correctly, if every encounter between the electron and the cation led to recombination. However, quite the opposite is the case. Most of the time, the ion−ion encounters are unreactive and only ion-pairs, $(e_{am}^-\cdot NH_4^+)$, are transiently formed. The solvated electron and the ammonium cation diffuse as a pair without neutralizing and disappearing as ammonia molecules and hydrogen atoms. The actual recombination occurs only at the instant, when the ion-pair finally meets with the dipole. Thus, one would severely overestimate the ejection length from fitting the experimentally observable escape probability with eq 6. This is easily seen by introducing the geminate electron−ion recombination probability, W_∞^{ion}, or the probability for ion-pair formation

$$W_\infty^{ion}(r_0) = 1 - \Omega_\infty^{ion}(r_0) \tag{7}$$

where r_0 is the initial separation at the instant of solvated electron generation. If every ion−ion encounter would directly lead to solvated electron annihilation, the ion-pair dissociation probability, Ω_∞^{ion}, would be equal to the measured escape probability, Ω_∞. This is, however, not the case because the ion-pair itself needs to encounter the amidogen radical before the solvated electron is lost. Since the ion-pair itself represents a strongly bound dipole, its reaction with the NH_2 dipole can be regarded as a dipole−dipole recombination, which can be treated in the framework of the neutral pair approximation[95] where any electrostatic interaction between the reaction partners is neglected. In this case, the probability for geminate recombination is simply given by the ratio of the reaction distance to the initial dipole−dipole distance

$$W_\infty^{dip}(r_1) = R/r_1 \tag{8}$$

In our case, the reaction distance, R, takes into account the finite separation between the dipoles at which their reaction occurs, while the dipole−dipole distance, r_1, is equal to the separation between the ion-pair, $(e_{am}^-\cdot NH_4^+)$, and the NH_2 dipole at the instant when the ion-pair is formed. As the annihilation occurs diffusion-controlled, the ultimate recombination probability is then given by the probability for the ion-pair formation multiplied by the dipole−dipole reaction probability, i.e.,

$$W_\infty^{total}(r_0, r_1) = W_\infty^{ion}(r_0) W_\infty^{dip}(r_1) \tag{9}$$

and the ultimate escape probability seen experimentally then becomes

$$\Omega_\infty^{total}(r_0, r_1) = 1 - W_\infty^{ion}(r_0) W_\infty^{dip}(r_1) \tag{10}$$

In principle, as with eq 6, an averaging over the distribution of initial ion−ion distances would have to be carried out. Furthermore, because of the diffusive nature of the relative approach between the ion-pair and the NH_2 radical, a distribution of dipole−dipole distances will be established in solution over which an additional averaging is in principle also required. For simplicity, this effect of the diffusional spreading of the radial dipole pair distribution will be neglected as will be the influence of the distribution of ejection lengths.

The transient existence of the ion-pair introduces two additional parameters to the model, namely, the dipole−dipole reaction radius, R, and the initial dipole−dipole distance, r_1. The former quantity has been determined by Kieffer et al. from pulse radiolysis experiments to 5.8 Å at a temperature of 223 K.[52] No temperature dependence of this quantity has been reported so far, and we therefore assume it to be constant throughout the thermodynamic range studied here. The initial dipole−dipole separation, r_1, can be approximated as the average distance, $r_{NH_4^+}$, traveled by the ammonium cation relative to the radical during the time period between the initial photoionization and the ion-pair formation (see Figure 8). Similarly, an average distance, r_{e^-}, migrated by the solvated electron during that time window can also be defined. The ejection length is then simply given by the sum of the two electrostatic drift distances, $r_0 = r_{NH_4^+} + r_{e^-}$. Since the distance ratio, $r_{e^-}/(r_{NH_4^+})$, can be expressed by the ratio of the particles' diffusion constants, $D_{e^-}/D_{NH_4^+}$, the initial dipole−dipole separation is obtained in the form

$$r_1 = \frac{D_{NH_4^+}}{D_{NH_4^+} + D_{e^-}} r_0 \tag{11}$$

Once again, we reiterate that the diffusional nature of the particle motions will lead to a spatial spreading of the density distributions with time, which can be dealt with optimally by numerically solving the relevant Smoluchowski diffusion equations[35,41,93,96,97] or by means of Monte Carlo simulations.[41,98,99] At this stage, it suffices to use eq 11 for estimating the relative distances between the peaks of the density distributions of the recombining particles.

The diffusion coefficient of the solvated electron is 1.5 Å^2/ps at 223 K, while at the same temperature, those of the ammonium cation and the amidogen radical are only 0.23 Å^2/ps and 0.5 Å^2/ps, respectively.[80] Therefore, the collisional dynamics of the recombining particles in the liquid solvent are dominated by the mobility of the solvated electron. Since no information is available regarding the temperature and density dependencies of the diffusion coefficients, we assume that they scale identically with the T- and ρ-dependent diffusivity of the neat solvent. In that case, the ratio of r_1 to r_0 remains constant (see eq 11), and the only fitting parameter in the model is again the thermalization distance (cf. Figure 8).

dx.doi.org/10.1021/jp211725r | J. Phys. Chem. B 2012, 116, 2223−2233

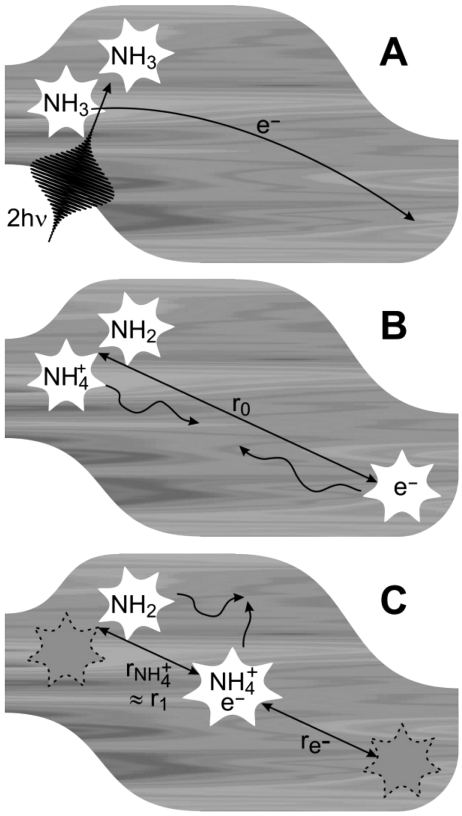

Figure 8. Sketch of the recombination dynamics relevant to the ammoniated electron. (A) The 2-photon ionization generates solvated electrons at the thermalization distance, r_0, from the ionization site. (B) The ammonium cation and the solvated electron drift toward each other in their mutual Coulomb field to form the ion-pair. (C) The ion-pair is created at the average distance, r_1, from the initial ionization site, which can be estimated from the diffusion coefficients of the two independently diffusing particles.

Figure 9 shows a comparison of the experimental survival probabilities with the Onsager model that is extended to describe the ion-pair-mediated electron dipole recombination. The most important difference to the unmodified model (cf. Figure 7) is that indeed for the same thermodynamic conditions, significantly smaller thermalization distances are required to obtain the same escape yield. Whereas the unmodified Onsager model (eq 6) suggested an ejection length of ∼12 nm, a satisfactory fit is now obtained with $\langle r_0 \rangle = r_0 = 6.6$ nm. This value is still perfectly consistent with an ionization mechanism that creates the electrons transiently in the conduction band of the solvent. For the hydrated electron generated photolytically above the band gap,[31,62,100] a thermalization distance of 4 nm was determined thereby confirming a previous report that quasi-free electrons are slightly more mobile in ammonia as compared to water.[77]

Finally, Figure 9 reveals that the escape probability does not vanish when the product, $\varepsilon(T,\rho)T$, approaches zero. According to eq 10, the escape probability assumes a value of $\Omega_\infty^{\text{total}} = 1 - R/r_1$ in the limit $\varepsilon(T,\rho)T \to 0$. In other words, regardless of the solvent screening, the solvated electron can only be quantitatively annihilated in a configuration where the ion-pair is generated within the reaction radius for its recombination with the dipole. The finite intercept leads to a considerably bent model prediction in the linearized representation (Figure 9, bottom panel). Therefore, the curved behavior of the experimental

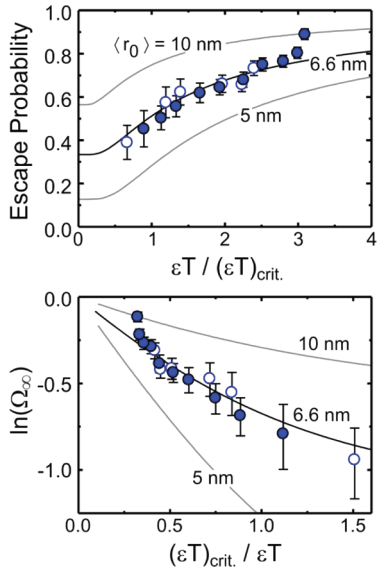

Figure 9. Comparison of the extended Onsager model with experimental escape probabilities of the solvated electron in liquid-to-supercritical ammonia (filled circles, isobaric at 300 bar; open circles, isothermal at 423 K).

data that we already noticed in Figure 7 can at least partially be attributed to the sequential nature of the recombination mechanism. Unfortunately, the accuracy of our data is currently not good enough to decide whether or not the ejection length depends on the temperature and the density. Here, it seems as if the assumption of a constant thermalization distance from the compressed liquid to the dilute supercritical fluid is sufficiently accurate. We are currently engaged in numerical Monte Carlo simulations to provide a more sophisticated molecular level description of the effect of ion-pair formation on the geminate recombination dynamics of the ammoniated electron. These simulations will also serve as a basis for a detailed analysis of the apparent recombination kinetics, a subject whose discussion is postponed to a forthcoming publication.

CONCLUSIONS

In summary, we have investigated for the first time the initial recombination of photolytically generated solvated electrons in liquid and supercritical ammonia. The mechanism creating the ammoniated electron relies on an initial two-photon ionization with a transient formation of electrons in the conduction band of the solvent. The conduction band electrons feature a high mobility thereby resulting in a thermalization distance that is much larger than that of solvated electrons generated at comparable ionization energies from water where the conduction band is energetically not accessible. Because of the large ejection length, the geminate escape probability is surprisingly high. The dependence of the escape yields on the thermodynamic state variables, temperature, density, and dielectric constant has been explored in a systematic fashion and was found to be in remarkable agreement with the theoretical predictions from the classical Onsager model for the initial recombination of ions. Within the accuracy of the experimental data there is no need to invoke a temperature and density dependent thermalization distance. The Onsager model was further refined to account for the transient appearance of the ammonium−electron ion-pairs, which diffusively migrate in the liquid solution in a correlated manner. While the reactant motions are governed by the

dx.doi.org/10.1021/jp211725r | J. Phys. Chem. B 2012, 116, 2223−2233

electrostatic drift of the electron toward the ammonium cation and the ion-pair formation, the reactivity of the solvated electron is dictated by the reactivity of the ion-pair toward the amidogen radical. We therefore speak of an ion-pair-mediated electron-dipole recombination. Future experiments of the multiphoton ionization of liquid-to-supercritical amines and aminoalcohols are currently underway in our laboratories to further unravel specifically the role of hydrogen-bonding for the recombination dynamics of solvated electrons in condensed phases. To explore the thermalization dynamics prior to electron recombination, additional experiments with tunable probe pulses will be carried out. In addition, we are planning to conduct experiments on the geminate recombination of electrons with NH_2 in the absence of the cation following a photodetachment of the electron by charge transfer to solvent excitation of amide anions in the ultraviolet. Finally, multiple pulse experiments including photolysis-pump−probe spectroscopy are targeted at comparing the relaxation dynamics of photolytically generated solvated electrons with those from our previous studies on solvated electrons from metal−ammonia solutions. Such a comparison might prove very helpful in exploring the solvated electron's mode of binding to the medium and its time-dependent changes during the localization dynamics, i.e., as the highly mobile conduction band electron becomes trapped and fully thermalized at a local solvent site.

AUTHOR INFORMATION

Corresponding Author

*E-mail: p.voehringer@uni-bonn.de.

Notes

The authors declare no competing financial interest.

ACKNOWLEDGMENTS

Financial support by the Deutsche Forschungsgemeinschaft through the Collaborative Research Center, SFB 813 "Chemistry at Spin Centers", and through project VO 593/6-1 is gratefully acknowledged. We are furthermore indebted to Professor Dirk Schwarzer for continued support and inspiring discussion.

REFERENCES

(1) Mozumder, A. *Fundamentals of Radiation Chemistry*; Academic Press: San Diego, 1999.
(2) Hart, E. J.; Anbar, M. *The Hydrated Electron*; John Wiley & Sons Inc.: New York, 1970.
(3) Zurek, E.; Edwards, P. P.; Hoffmann, R. *Angew. Chem., Int. Ed.* **2009**, *48*, 8198.
(4) Larsen, R. E.; Glover, W. J.; Schwartz, B. J. *Science* **2010**, *329*, 65.
(5) Haberland, H.; Ludewigt, C.; Schindler, H.-G.; Worsnop, D. R. *Surf. Sci.* **1985**, *156* (Part 1), 157.
(6) Lee, G. H.; Arnold, S. T.; Eaton, J. G.; Sarkas, H. W.; Bowen, K. H.; Haberland, H. *Z. Phys. D* **1991**, *20*, 9.
(7) Sarkas, H. W.; Arnold, S. T.; Eaton, J. G.; Lee, G. H.; Bowen, K. H. *J. Chem. Phys.* **2002**, *116*, 5731.
(8) Hertel, I. V.; Huglin, C.; Nitsch, C.; Schulz, C. P. *Phys. Rev. Lett.* **1991**, *67*, 1767.
(9) Schulz, C. P.; Gerber, A.; Nitsch, C.; Hertel, I. V. *Z. Phys. D* **1991**, *20*, 65.
(10) Stert, V.; Radloff, W.; Schulz, C. P.; Hertel, I. V. *Eur. Phys. J. D* **1999**, *5*, 97.
(11) Schulz, C. P.; Scholz, A.; Hertel, I. V. *Isr. J. Chem.* **2004**, *44*, 19.
(12) Lee, I.-R.; Lee, W.; Zewail, A. H. *ChemPhysChem* **2008**, *9*, 83.
(13) Huppert, D.; Rentzepis, P. M.; Struve, W. S. *J. Phys. Chem.* **1975**, *79*, 2850.
(14) Belloni, J.; Clerc, M.; Goujon, P.; Saito, E. *J. Phys. Chem.* **1975**, *79*, 2848.
(15) Lindner, J.; Unterreiner, A. N.; Vöhringer, P. *ChemPhysChem* **2006**, *7*, 363.
(16) Lindner, J.; Unterreiner, A.-N.; Vöhringer, P. *J. Chem. Phys.* **2008**, *129*, 064514.
(17) Jortner, J. *J. Chem. Phys.* **1959**, *30*, 839.
(18) Barnett, R. N.; Landman, U.; Cleveland, C. L.; Kestner, N. R.; Jortner, J. *Chem. Phys. Lett.* **1988**, *148*, 249.
(19) Barnett, R. N.; Landman, U.; Cleveland, C. L.; Kestner, N. R.; Jortner, J. *J. Chem. Phys.* **1988**, *88*, 6670.
(20) Marchi, M.; Sprik, M.; Klein, M. L. *J. Chem. Phys.* **1988**, *89*, 4918.
(21) Sprik, M.; Klein, M. L. *J. Chem. Phys.* **1988**, *89*, 1592.
(22) Sprik, M.; Impey, R. W.; Klein, M. L. *J. Chem. Phys.* **1985**, *83*, 5802.
(23) Barnett, R. N.; Landman, U.; Nitzan, A. *Phys. Rev. Lett.* **1989**, *62*, 106.
(24) Sprik, M.; Klein, M. L. *J. Chem. Phys.* **1989**, *91*, 5665.
(25) Sprik, M.; Klein, M. L. *J. Chem. Phys.* **1989**, *90*, 7614.
(26) Marchi, M.; Sprik, M.; Klein, M. L. *Faraday Discuss. Chem. Soc.* **1988**, *85*, 373.
(27) Shkrob, I. A. *J. Phys. Chem. A* **2006**, *110*, 3967.
(28) Migus, A.; Gauduel, Y.; Martin, J. L.; Antonetti, A. *Phys. Rev. Lett.* **1987**, *58*, 1559.
(29) Long, F. H.; Lu, H.; Eisenthal, K. B. *Phys. Rev. Lett.* **1990**, *64*, 1469.
(30) Sander, M. U.; Luther, K.; Troe, J. *J. Phys. Chem.* **1993**, *97*, 11489.
(31) Crowell, R. A.; Bartels, D. M. *J. Phys. Chem.* **1996**, *100*, 17940.
(32) Hertwig, A.; Hippler, H.; Unterreiner, A. N.; Vöhringer, P. *Ber. Bunsenges. Phys. Chem.* **1998**, *102*, 805.
(33) Assel, M.; Laenen, R.; Laubereau, A. *J. Phys. Chem. A* **1998**, *102*, 2256.
(34) Hertwig, A.; Hippler, H.; Unterreiner, A. N. *Phys. Chem. Chem. Phys.* **1999**, *1*, 5633.
(35) Madsen, D.; Thomsen, C. L.; Thogersen, J.; Keiding, S. R. *J. Chem. Phys.* **2000**, *113*, 1126.
(36) Elles, C. G.; Jailaubekov, A. E.; Crowell, R. A.; Bradforth, S. E. *J. Chem. Phys.* **2006**, *125*, 044515.
(37) Elles, C. G.; Shkrob, I. A.; Crowell, R. A.; Bradforth, S. E. *J. Chem. Phys.* **2007**, *126*, 164503.
(38) Petersen, C.; Thogersen, J.; Jensen, S. K.; Keiding, S. R. *J. Phys. Chem. A* **2007**, *111*, 11410.
(39) Kratz, S.; Torres-Alacan, J.; Urbanek, J.; Lindner, J.; Vöhringer, P. *Phys. Chem. Chem. Phys.* **2010**, *12*, 12169.
(40) Iglev, H.; Fischer, M. K.; Rossmadl, H. *J. Chem. Phys.* **2011**, *134*, 214507.
(41) Torres-Alacan, J.; Kratz, S.; Vöhringer, P. *Phys. Chem. Chem. Phys.* **2011**, *13*, 20806.
(42) Onsager, L. *Phys. Rev.* **1938**, *54*, 554.
(43) PROPATH Group. *PROPATH: A Program Package for Thermophysical Properties*, version 13.1, 2008.
(44) Buback, M.; Harder, W. D. *Ber. Bunsenges. Phys. Chem.* **1977**, *81*, 609.
(45) Schäfer, T.; Lindner, J.; Vöhringer, P.; Schwarzer, D. *J. Chem. Phys.* **2009**, *130*, 224502.
(46) Schäfer, T.; Schwarzer, D.; Lindner, J.; Vöhringer, P. *J. Chem. Phys.* **2008**, *128*, 064502.
(47) Schwarzer, D.; Lindner, J.; Vöhringer, P. *J. Phys. Chem. A* **2006**, *110*, 2858.
(48) Vogelsgesang, R.; Schindewolf, U. *Ber. Bunsenges. Phys. Chem* **1971**, *75*, 651.
(49) Olinger, R.; Schindewolf, U. *Ber. Bunsenges. Phys. Chem* **1971**, *75*, 690.
(50) Olinger, R.; Schindewolf, U.; Hahne, S. *Ber. Bunsenges. Phys. Chem.* **1972**, *76*, 349.
(51) Koehler, W. H.; Lagowski, J. J. *J. Phys. Chem.* **1969**, *73*, 2329.

(52) Kieffer, F.; Klein, J.; Lapersonne-Meyer, C.; Magat, M.; Belloni, J.; Billiau, F.; Cordier, F.; Delaire, J.; Delcourt, M. O. *Faraday Discuss. Chem. Soc.* **1977**, *63*, 55.
(53) Belloni, J.; Cordier, P.; Delaire, J. *Chem. Phys. Lett.* **1974**, *27*, 241.
(54) Belloni, J.; Billiau, F.; Cordier, P.; Delaire, J. A.; Delcourt, M. O. *J. Phys. Chem.* **1978**, *82*, 532.
(55) Farhataziz; Perkey, L. M.; Hentz, R. R. *J. Chem. Phys.* **1974**, *60*, 4383.
(56) Williams, F.; Varma, S. P.; Hillenius, S. *J. Chem. Phys.* **1976**, *64*, 1549.
(57) Krohn, C. E.; Thompson, J. C. *Phys. Rev. B* **1979**, *20*, 4365.
(58) Coe, J. V.; Earhart, A. D.; Cohen, M. H.; Hoffman, G. J.; Sarkas, H. W.; Bowen, K. H. *J. Chem. Phys.* **1997**, *107*, 6023.
(59) Elles, C. G.; Rivera, C. A.; Zhang, Y.; Pieniazek, P. A.; Bradforth, S. E. *J. Chem. Phys.* **2009**, *130*, 084501.
(60) Winter, B.; Weber, R.; Widdra, W.; Dittmar, M.; Faubel, M.; Hertel, I. V. *J. Phys. Chem. A* **2004**, *108*, 2625.
(61) Nordlund, D.; Ogasawara, H.; Bluhm, H.; Takahashi, O.; Odelius, M.; Nagasono, M.; Pettersson, L. G. M.; Nilsson, A. *Phys. Rev. Lett.* **2007**, *99*, 217406.
(62) Son, D. H.; Kambhampati, P.; Kee, T. W.; Barbara, P. F. *J. Phys. Chem. A* **2001**, *105*, 8269.
(63) Son, D. H.; Kambhampati, P.; Kee, T. W.; Barbara, P. F. *Chem. Phys. Lett.* **2001**, *342*, 571.
(64) Boyle, J. W.; Ghormley, J. A.; Hochanadel, C. J.; Riley, J. R. *J. Phys. Chem.* **1969**, *73*, 2886.
(65) Bartels, D. M.; Crowell, R. A. *J. Phys. Chem. A* **2000**, *104*, 3349.
(66) Ashfold, M. N. R.; Langford, S. R.; Morgan, R. A.; Orr-Ewing, A. J.; Western, C. M.; Scheper, C. R.; de Lange, C. A. *Eur. Phys. J. D* **1998**, *4*, 189.
(67) Walsh, A. D.; Warsop, P. A. *Trans. Faraday Soc.* **1961**, *57*, 345.
(68) Douglas, A. E. *Discuss. Faraday Soc.* **1963**, *35*, 158.
(69) Ashfold, M. N. R.; Bennett, C. L.; Dixon, R. N. *Chem. Phys.* **1985**, *93*, 293.
(70) Banna, M. S.; Shirley, D. A. *J. Chem. Phys.* **1975**, *63*, 4759.
(71) Rabalais, J. W.; Karlsson, L.; Werme, L. O.; Bergmark, T.; Siegbahn, K. *J. Chem. Phys.* **1973**, *58*, 3370.
(72) Locht, R.; Leyh, B.; Denzer, W.; Hagenow, G.; Baumgärtel, H. *Chem. Phys.* **1991**, *155*, 407.
(73) Almeida, T. S.; Coutinho, K.; Cabral, B. J. C.; Canuto, S. *J. Chem. Phys.* **2008**, *128*, 014506.
(74) Lindblad, A.; Bergersen, H.; Pokapanich, W.; Tchaplyguine, M.; Ohrwall, G.; Bjorneholm, O. *Phys. Chem. Chem. Phys.* **2009**, *11*, 1758.
(75) Krohn, C. E.; Antoniewicz, P. R.; Thompson, J. C. *Surf. Sci.* **1980**, *101*, 241.
(76) Huntress, W. T.; Mosesman, M. M.; Elleman, D. D. *J. Chem. Phys.* **1971**, *54*, 843.
(77) Krebs, P. *J. Phys. Chem.* **1984**, *88*, 3702.
(78) Farhataziz; Perkey, L. M.; Hentz, R. R. *J. Chem. Phys.* **1974**, *60*, 717.
(79) Farhataziz; Perkey, L. M. *J. Phys. Chem.* **1975**, *79*, 1651.
(80) Belloni, J.; Cordier, P.; Delaire, J. A.; Delcourt, M. O. *J. Phys. Chem.* **1978**, *82*, 537.
(81) Fletcher, J. W.; Seddon, W. A. *Faraday Discuss.* **1977**, *63*, 18.
(82) Seddon, W. A.; Fletcher, J. W.; Sopchyshyn, F. C.; Jevcak, J. *Can. J. Chem.* **1974**, *52*, 3269.
(83) Dye, J. L.; Debacker, M. G.; Dorfman, L. M. *J. Chem. Phys.* **1970**, *52*, 6251.
(84) Belloni, J.; Billiau, F.; Delaire, J. A.; Delcourt, M. O.; Marignier, J. L. *Radiat. Phys. Chem.* **1983**, *21*, 177.
(85) Brooks, J. M.; Dewald, R. R. *J. Phys. Chem.* **1971**, *75*, 986.
(86) Schindewolf, U. *Ber. Bunsenges. Phys. Chem.* **1982**, *86*, 887.
(87) Buxton, G. V. In *Radiation Chemistry: Present Status and Future Trends*; Jonah, C. D., Rao, B. S. M., Eds.; Elsevier: Amsterdam, The Netherlands, 2001; p 145.
(88) Rubinstein, G.; Tuttle, T. R.; Golden, S. *J. Phys. Chem.* **1973**, *77*, 2872.
(89) Jou, F.-Y.; Freeman, G. R. *J. Phys. Chem.* **1981**, *85*, 629.
(90) Sano, H.; Tachiya, M. *J. Chem. Phys.* **1979**, *71*, 1276.
(91) Tachiya, M. *J. Chem. Phys.* **1988**, *89*, 6929.
(92) Wojcik, M.; Tachiya, M. *J. Chem. Phys.* **2009**, *130*, 104107.
(93) Thomsen, C. L.; Madsen, D.; Keiding, S. R.; Thøgersen, J.; Christiansen, O. *J. Chem. Phys.* **1999**, *110*, 3453.
(94) Egorov, S. A.; Yethiraj, A.; Skinner, J. L. *Chem. Phys. Lett.* **2000**, *317*, 558.
(95) Collins, F. C.; Kimball, G. E. *J. Colloid Sci.* **1949**, *4*, 425.
(96) Pimblott, S. M. *J. Phys. Chem.* **1991**, *95*, 6946.
(97) Green, N. J. B.; Pilling, M. J.; Pimblott, S. M.; Clifford, P. *J. Phys. Chem.* **1990**, *94*, 251.
(98) Cobut, V.; Frongillo, Y.; Patau, J. P.; Goulet, T.; Fraser, M. J.; Jay-Gerin, J. P. *Radiat. Phys. Chem.* **1998**, *51*, 229.
(99) Frongillo, Y.; Goulet, T.; Fraser, M. J.; Cobut, V.; Patau, J. P.; Jay-Gerin, J. P. *Radiat. Phys. Chem.* **1998**, *51*, 245.
(100) Sander, M. U.; Luther, K.; Troe, J. *Ber. Bunsenges. Phys. Chem.* **1993**, *97*, 953.